Journal of Materials Chemistry C

ROYAL SOCIETY OF CHEMISTRY

PAPER

View Article Online
View Journal

Cite this: DOI: 10.1039/d5tc03809j

The magic of semi-perfluorinated mixtures: engineering MR-TADF emission from host–guest mixtures of liquid crystals

Julius A. Knöller,[a] Tobias Günther,[a] Tomas Matulaitis,[b] Anna Zens,[a] Eli Zysman-Colman *[b] and Sabine Laschat *[a]

Received 23rd October 2025,
Accepted 8th December 2025

DOI: 10.1039/d5tc03809j

rsc.li/materials-c

Two liquid crystalline emitter–host mixtures have been developed, where each of the emitter and host self-assembles into a columnar hexagonal (Col_h) mesophase, as does the mixture. The emitter consists of a modified 7-(*tert*-butyl)-5-oxa-8*b*-aza-15*b*-bora-benzo[*a*]naphtho[1,2,3-*hi*]-aceanthrylene **B–O–Cz** multi-resonant thermally activated delayed fluorescence (MR-TADF) core containing lateral semiperfluorinated side chains, while the host is derived from a modified MR-TADF 5,9-dioxa-13*b*-boranaphtho[3,2,1-*de*]anthracene (DOBNA) core that also contains lateral semiperfluorinated side chains. Unlike the previously used alkoxy side chains in TADF liquid crystalline materials, the semiperfluorinated side chains only minimally perturb the optoelectronic properties of the luminescent cores, this despite the strong aggregation within the ordered columnar hexagonal (Col_{ho}) phase. This was achieved by shielding the emitter moieties from each other within the host mesophase, which mitigates excimer emission from aggregates and by engineering an efficient Förster resonance energy transfer from the host material to the emitter in the blend.

Introduction

Emissive liquid crystals (LCs) are attractive materials for various applications such as organic light-emitting diodes (OLEDs), organic field effect transistors (OFETs), organic photovoltaic devices (OPVs),[1,2] linear polarized emission,[3] and luminescent concentrators,[4] among others.[5] In particular, discotic LCs are promising in that respect. The strong π–π interactions of their (hetero)aromatic cores and van der Waals interactions of the flexible side chains promote self-assembly into columnar mesophases with long-range orientational order,[5–10] resulting in increased charge carrier mobility along the columnar axis.[11] Moreover, the electronic properties of the (hetero)aryl core can be tailored so that either hole or electron-conducting materials are obtained. Functionalization of the (hetero)aryl core leads to improved solution processability.[11–14] Further advantages are the self-healing of defects through the local fluidity of the molecules within the mesophase.[5,6,9] An important parameter for OLEDs is the alignment of the emitter, which is frequently correlated with the orientation of the transition dipole moment that controls the light outcoupling. The alignment of the molecule can be controlled by the type of columnar mesophase (*i.e.*, hexagonal or rectangular)[7] or surface nanopatterning,[15] and monitored by 4D scanning tunneling electron microscopy (STEM).[16] This results in controlled alignment of transition dipoles.[14,17] For OLEDs to be efficient, the device must harvest both singlet and triplet excitons to produce light, typically managed by the emissive material. One possible solution is LC emitters that are thermally activated delayed fluorescent (TADF).[18,19] TADF emitters possess a small singlet–triplet energy gap (ΔE_{ST}), enabling the thermal upconversion of triplet excitons into singlets by reverse intersystem crossing (RISC), thus permitting up to 100% of the excitons to be converted into light in the device.[18,19]

Several TADF-LCs have been reported (Fig. 1), such as carbazole-benzonitrile donor–acceptor (D–A)–TADF compounds **1a–c** displaying columnar hexagonal (Col_h) mesophases.[12,13] the substitution pattern and symmetry have a strong impact on the photophysical properties. For example, quantum yields Φ decreased from 11% (for **1b**) to 1.5% (for **1c**) despite the small singlet–triplet gaps ΔE_{ST} of 0.01 and 0.04eV, respectively. In addition, several TADF emitters that self-assemble into lamellar phases have been reported[11,17] (for details see SI, Fig. S64 and discussion).

A 1 : 1 mixture of columnar DOBNA derivative **2a** (Y = B) and its N-analogue **2b** (Y = N) forms a supramolecular copolymer *via* B–N frustrated Lewis pairs.[20] The copolymer showed yellow emission in decaline (λ_{PL} = 550 nm; τ_p = 96 ns, τ_d = 6 μs) and

[a] *Institut für Organische Chemie, Universität Stuttgart, Pfaffenwaldring 55, D-70569 Stuttgart, Germany. E-mail: sabine.laschat@oc.uni-stuttgart.de*
[b] *Organic Semiconductor Centre, EaStCHEM School of Chemistry, University of St Andrews, St Andrews, Fife KY16 9ST, UK. E-mail: eli.zysman-colman@st-andrews.ac.uk*

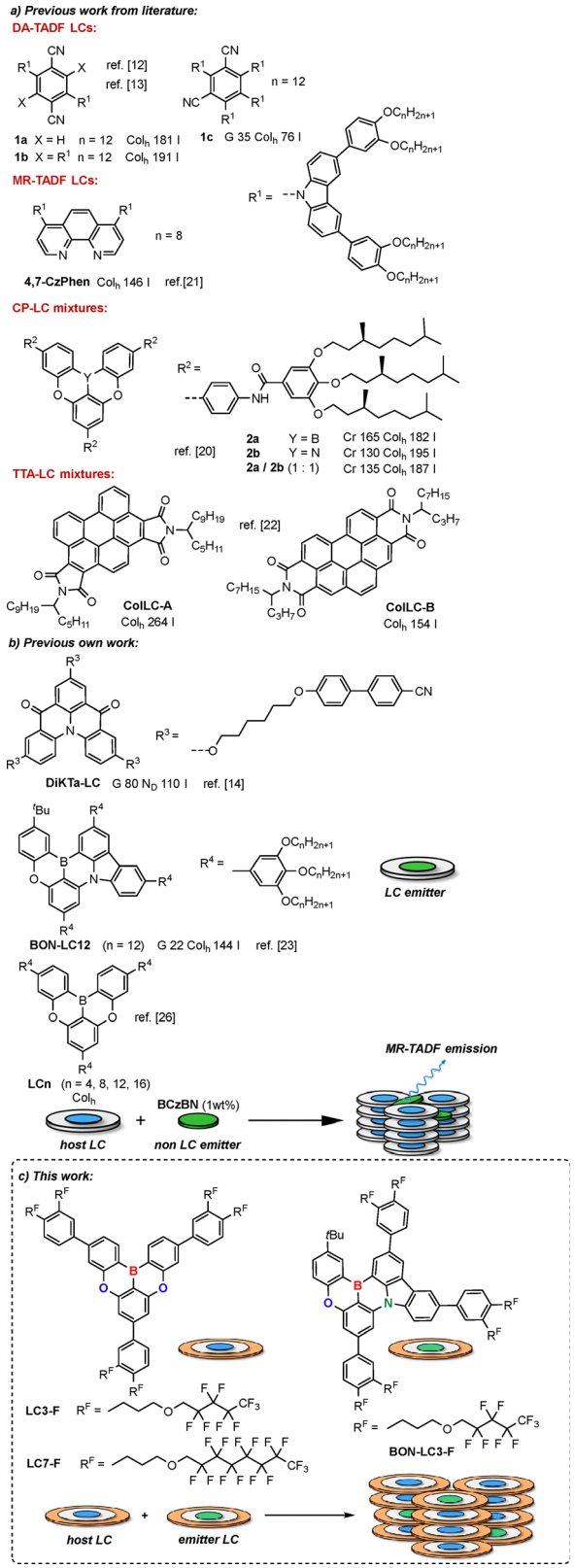

Fig. 1 Overview of literature-known TADF-LCs; (b) our previous work on MR-TADF LCs (**DiKTaLC**, **BON-LC**, **LCn**); (c) our new strategy towards liquid crystalline emitter host mixtures features MR-TADF emission at room temperature.

circular polarized emission (λ_{PL} = 550 nm, g_{PL} = 7 × 10^{-3}). Very recently, the dual fluorescent dye **4,7-CzPhen** consisting of phenanthroline with two peripheral carbazole units, was reported, which showed broad Col_h mesophases already at ambient temperature.[21] The substitution pattern controlled the photophysical properties. Within the series of regioisomers, only **4,7-CzPhen** displayed TADF in PS matrix (≪1 wt%) (Φ_{PL} = 25%). Columnar self-assembly of perylene imides **ColLC-A**, **ColLC-B** led to mesophase-assisted aggregation-induced delayed fluorescence (AIDF) by triplet–triplet annihilation.[22] While the large ΔE_{ST} = 0.83, 1.16 eV, respectively, precluded TADF emission, the close contact of the stacked molecules of the two different mesogens in the Col_h phase promoted delayed fluorescence by triplet–triplet annihilation (TTA) from imide aggregates (*i.e.*, **ColLC-A**), assisted by energy transfer from the imidoester **ColLC-B** (Φ_{PL} = 37%). All blends show similar emission (λ_{PL} = 575 nm, Φ_{PL} = 16% for 1 : 1 blend) as neat **ColLC-A** (Φ_{PL} = 17%). OLEDs with **ColLC-A** showed EQE_{max} = 1.8%.[22]

However, the strong intermolecular interactions governing LC self-assembly impair the photophysical properties. For example, the formation of columnar stacks of emitter molecules often leads to aggregation-caused quenching (ACQ) and thus the Φ_{PL} is significantly reduced in the liquid crystalline bulk phase as compared to in solution.[11–14,17,23] To address this challenge, one strategy involves designing TADF-LC materials that self-assemble into lower-order structures. Therefore, we developed **DiKTaLC** (Fig. 1), a nematic discotic (N_D) LC having a ΔE_{ST} of 0.20 eV.[14] Neat thin films showed green emission (λ_{PL} = 512 nm, Φ_{PL} = 52%, τ_p = 7 ns, τ_d = 70.2 μs). Comparison with the non-mesogenic counterpart revealed that the mesogenic 4-cyanobiphenyl units control the emitter orientation, resulting in homeotropic alignment in thin films and a preferentially horizontally aligned TDM. Doped blue-green emitting OLEDs (λ_{PL} = 492 nm) with **DiKTaLC** showed an EQE_{max} of 13.6%.[14]

A second common approach to reduce excimer formation utilizes doping of the TADF-LC emitter (1–20 wt%) into a low molecular weight or polymeric host material,[11–14,17,23] a strategy that is also employed for non-LC emitters.[24,25] For example, **BON-LC12** self-assembles into a broad Col_h phases (Fig. 1), which is stable even at sub-ambient temperatures. However, the strong interactions in the neat Col_h mesophase suppressed TADF emission.[23] In contrast, when **BON-LC12** was diluted into a polystyrene host matrix (1 wt% **BON-LC12**), TADF emission is observed (λ_{PL} = 467 nm, Φ_{PL} = 90%, τ_p = 9.85 ns, τ_d = 107.9 μs).[23]

Despite the improved photophysical properties, in most cases, such host–guest mixtures no longer show any LC behavior, which effectively defeats the purpose of incorporating the mesogenic units.[11] Recently, we disclosed host–emitter mixtures consisting of a columnar DOBNA host **LCn**[26] and a non-mesogenic "disk-like" MR-TADF emitter **BCzBN**,[27] where the columnar mesophase of the host was maintained in the mixture, enabling efficient Förster resonance energy transfer (FRET) from the LC host to the emitter, and thus, narrowband MR-TADF emission (*e.g.* **LC8**/**BCzBN**: λ_{PL} = 476 nm, Φ_{PL} = 41%, τ_p = 8.19 ns, τ_d = 108.5 μs), was observed, even in the tightly

packed mesophases at room temperature.[26] The XRD data of the **LC8**/**BCzBN** mixtures in the Col_h mesophase suggest preferential localization of **BCzBN** in the aliphatic chain network.[26] While this arrangement is beneficial for photophysics alone (narrowband emission spectrum), it is not so helpful for controlling exciton dynamics.[19] Thus, the formation of mixed columnar stacks would be much more interesting. Unfortunately, mixing of **LCn** (as host) and **BON-LC** (as emitter) was not photophysically compatible due to the too low T_1 energy level of **LCn** (resulting from partial long-range charge transfer, LRCT, character of the emissive excited state due to the presence of the electron-rich alkoxy side groups). Thus, we wanted to implement alkyl-linked side chains on the central core to increase the T_1 energy of the host.

To minimize the electronic influence of the side chain on the emissive cores of both host and emitter, and to simultaneously enhance nanosegregation and thus promote liquid crystalline phase stability, we considered the use of semi-perfluorinated side chains instead of alkoxy chains as mesogenic groups attached to the MR-TADF core of the host and/or emitter, making use of the so-called fluorophobic effect.[28] The high polarity and low polarizability of C–F bonds lead to helical conformations of perfluorinated chains, and together with the larger size of F as compared to H, the lipophilicity and rigidity of the chains are increased.[28] It was shown for naphthalenetetracarboxylic diimide-derived organic transistors that the use of semi-perfluorinated side chains resulted in high mobility, and environmental and bias stress stability.[29] Improved transistor performance by fluorophobic self-organization was also reported for polymers with semi-perfluorinated side chains.[30,31] Moreover, the fluorophobic effect has been successfully exploited to induce and stabilize LC self-assembly.[32,33] Such an approach has yet to be used in TADF LC materials design.

Thus, here we designed columnar host–emitter LC mixtures showing MR-TADF emission in the columnar mesophase. We anticipated that the attachment of semiperfluorinated side chains on both host and emitter should facilitate LC self-assembly by fluorophobic interactions, while maintaining the singlet and triplet energy levels of the parent unsubstituted system. As the semi-perfluorinated side chains require more volume than alkoxy chains, only 6 instead of 9 side chains were attached in both hosts, **LC3-F**, **LC7-F**, and emitter **BON-LC3-F**, to avoid steric clashing that would perturb the self-assembly process. Our results demonstrate that this two-pronged approach indeed results in all columnar host–guest mixtures and enables FRET from the host to the emitter, resulting in narrowband MR-TADF emission.

Results and discussion

Theoretical studies

To understand the influence of the semi-perfluorinated alkyl chains on the hosts **LC3-F** and **LC7-F**, and the emitter **BON-LC3-F**, time-dependent density functional (TD-DFT) calculations at the PBE0/6-31G(d,p) level in the gas phase were carried out. Both hosts, **LC3-F** and **LC7-F**, have similar localizations of the HOMO and LUMO on the aromatic core (Fig. S1 and S2). The HOMO and LUMO are localized on alternating atoms, which is illustrative of a short-range charge transfer (SRCT) S_0–S_1 transition (HOMO–LUMO) that is typical of MR-TADF emitters.[34–36] As expected, the semi-perfluoroalkyl chains have very little influence on the HOMO and LUMO coefficients and energies. The HOMO (−5.75 eV) and LUMO (−1.64 eV) of the host **LC3-F** are slightly destabilized as compared to the HOMO (−5.81 eV) and LUMO (−1.70 eV) of the homologue **LC7-F** that has longer side chains, while the energy gap (E_g = 4.11 eV) remains identical. The energy values are slightly stabilized as compared to those of DOBNA derivatives containing alkoxy side chains, like **LC8** (HOMO−5.65 eV, LUMO−1.60 eV, E_g = 4.05 eV), reflecting the modest impact that the electronics of the mesogenic groups have on the energies of the frontier molecular orbitals.[26] Thus, we assumed that the MR-TADF character of the parent DOBNA system would be conserved in the derivatives containing semi-perfluorinated chains. Similarly, emitter **BON-LC3-F** possesses HOMO (−5.37 eV) and LUMO (−1.67 eV) levels that show the same alternating pattern of their electron density, and has an E_g = 3.70 eV, again in line with the SRCT character of the MR-TADF emitter **B-O-Cz** (Fig. S2). Comparison of **BON-LC3-F** with the known dodecyloxy-substituted derivative **BON-LC12**[23] revealed that the former has more stabilized orbitals than the latter (HOMO = −5.21 eV; LUMO = −1.67 eV; E_g = 3.54 eV for **BON-LC12**).

Synthesis of LC3-F, LC7-F and BON-LC3-F

The synthesis of host and emitter compounds commenced with the preparation of the semiperfluorinated side chains (Scheme 1). Williamson etherification of semiperfluorinated alcohols **4** with propargyl bromide **5** gave the ethers **6a**, **b**. Due to the high volatility of **6a**, it was used without isolation. In contrast, the corresponding higher homologue **6b** was obtained in 88% yield. Subsequent Sonogashira cross-coupling of ethers **6a**, **b** with 3,4-diiodobromobenzene **7** gave 3,4-bisalkinylbromobenzenes **8a**, **b** in 76 and 85% yield, which were then submitted to a sequential lithiation, borylation, and final catalytic hydrogenation of the triple bond to the pinacol borolanes **9a**, **b** carrying

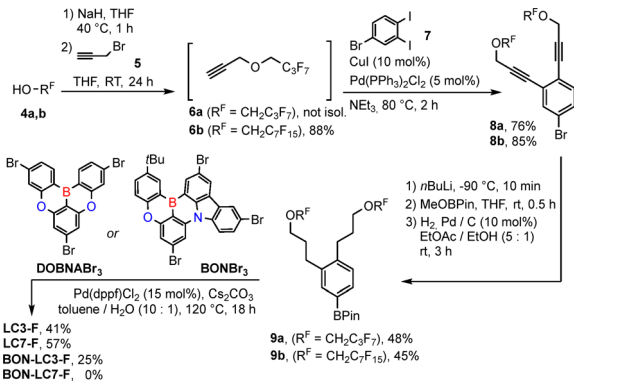

Scheme 1 Synthesis of hosts **LC3-F**, **LC7-F** and emitter **BON-LC3-F**.

semiperfluorinated alkyl chains in the 3,4-position in 48 and 45% yield over 3 steps.

Known **DOBNABr$_3$**[26] was treated with pinacol borolanes **9a, b** under Suzuki–Miyaura cross-coupling conditions to afford the desired hosts **LC3-F**, **LC7-F** in 41 and 57% yield, respectively. The corresponding Suzuki–Miyaura cross-coupling of known **BONBr$_3$**[23] gave the short-chain derivative **BON-LC3-F** in 25% yield, while the corresponding larger homologue **BON-LC7-F** could not be isolated due to severe solubility and purification issues.

Mesomorphic properties of LC3-F, LC7-F and BON-LC3-F

Upon cooling under the polarized optical microscope (POM), host **LC3-F** displayed large homeotropic areas with line defects (Fig. S42b) as well as fan-shaped textures (Fig. S42a), which were shearable and are characteristic of a columnar mesophase.[37–39] Similar POM textures were observed for the host **LC7-F**, also suggesting a columnar mesophase (Fig. S44).

In the 2nd heating cycle of the DSC of **LC3-F**, an endothermic clearing transition at 175.6 °C was detected (Fig. 2a and Table S2). Upon the 2nd cooling cycle, the isotropic phase to the Col$_{ho}$ transition was detected at 175.0 °C, and a glass transition was found at −68.6 °C. Thus, the phase range of the host **LC3-F** (ΔT = 244 K) is significantly broadened as compared to the DOBNA alkoxy derivative **LC8** (ΔT = 175 K),[26] and the Col$_h$ phase was stabilized (Fig. 2c). During the 2nd cooling cycle, **LC7-F** displayed a higher clearing point (237.1 °C) and a glass transition at −61.7 °C (Fig. S45a and Table S2), resulting in an expanded mesophase range (ΔT = 299 K), which is much broader compared to that of the alkoxy derivative **LC12** (ΔT = 106 K). These results demonstrate the stabilizing effect of the semiperfluorinated side chains resulting from the fluorophobic effect.[40,41]

In the WAXS, **LC3-F** showed four sharp reflections in the small-angle section and two diffuse wide-angle reflections, namely the halo caused by the distance of fluid-like semiperfluorinated side chains (d_{halo} = 5.07 A) and the π–π reflection caused by the intracolumnar distance ($d_{\pi-\pi}$ = 3.47 Å) (Fig. 3a and Table S3). The higher intensity and broad appearance of the halo can be explained by the higher electron density and layer space filling of the semiperfluorinated side chains as compared to the alkoxy side chains.[40,42,43] The sharp reflections of the SAXS (Fig. 3b) were assigned as (10), (11), (20), and (21) reflections of a Col$_{ho}$ phase (*p6mm*) due to their characteristic ratio of $1:1/\sqrt{3}:1/2:1/\sqrt{7}$. The small intensity of the (10) peak as compared to the higher order peaks (11), (20), (21) is probably caused by the high electron density of the semiperfluorinated side chain.[40,41,44]

The calculated molecular diameter of **LC3-F** d_{calc} = 31.6 Å is very similar to the experimentally observed lattice parameter a = 32.3 Å, indicating that only little interdigitation of the semiperfluorinated chains takes place. The longer homologue **LC7-F** displayed similar WAXS and SAXS behavior, and thus a Col$_{ho}$ phase (*p6mm*) with a = 40.5 Å and $d_{\pi-\pi}$ = 3.50 Å was assigned (Fig. S47 and Table S3).

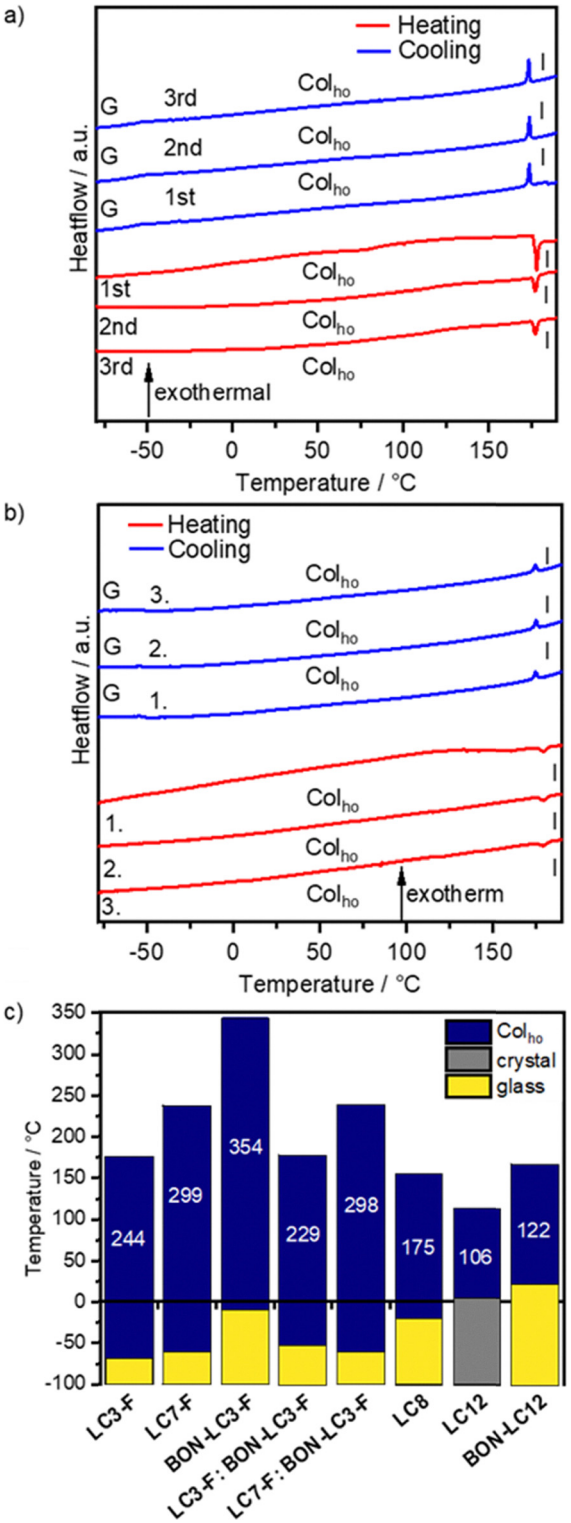

Fig. 2 (a) DSC thermogram (heating/cooling rate: 10 K min^{-1}) of compound **LC3-F**. G = glassy state, Col$_{ho}$: columnar hexagonally ordered mesophase, I = isotropic melt; (b) DSC thermogram (heating/cooling rate: 10 K min^{-1}) of **LC3-F** doped with 1 wt% of **BON-LC3-F**; (c) phase ranges of the semi-perfluorinated derivatives **LC3-F**, **LC7-F**, **BON-LC3-F** as well as mixtures **LC3-F** : **BON-LC3-F**, **LC7-F** : **BON-LC3** compared with the known alkoxy derivatives **LC8**, **LC12** and **BON-LC12** respectively, determined from the second cooling cycle of the DSC measurements. Values of **LC8**, **LC12**, **BON-LC12**, were taken from ref. 23 and 26 for comparison.

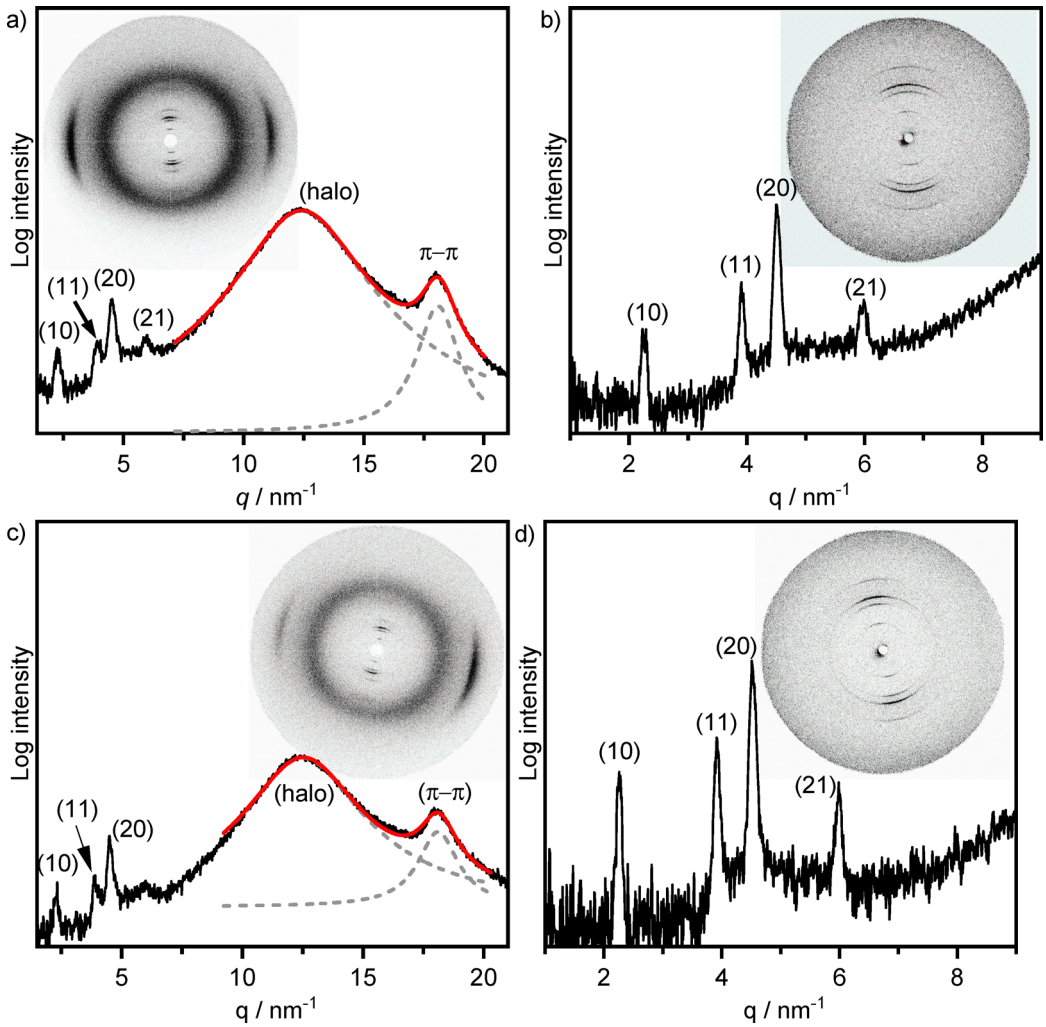

Fig. 3 (a) WAXS diffractogram of **LC3-F** recorded at 33 °C with the 2D WAXS pattern shown as inset. The red trace represents the fit of the wide-angle region with two Lorentzian functions (grey dashed traces); (b) SAXS diffractogram recorded at 33 °C with the 2D SAXS pattern shown as inset; (c) WAXS diffractogram of **LC3-F** doped with **BON-LC3-F** (1 wt%) recorded at 33 °C with the 2D WAXS pattern shown as inset. The red trace represents the fit of the wide-angle region with two Lorentzian functions (grey dashed traces); (d) SAXS diffractogram recorded at 33 °C with the 2D SAXS pattern shown as inset.

In contrast to the hosts **LC3-F** and **LC7-F**, the emitter **BON-LC3-F** showed only uncharacteristic textures under the POM (Fig. S43), which were shearable and thus indicative of a mesophase. As we anticipated potential problems with stability, transition temperatures, and enthalpies were extracted from the 1st heating and cooling cycle of the DSC. Upon the 1st cooling, **BON-LC3-F** displayed a clearing transition at 343.6 °C. Upon subsequent cooling, the mesophase reappeared at 343.6 °C, and a glass transition at −17.5 °C was detected, resulting in a large phase width (ΔT = 364 K, Fig. S45b and Table S2). In the WAXS, at 116 °C, **BON-LC3-F** displayed three distinct small-angle reflections and two diffuse wide-angle reflections, *i.e.*, the halo (d_{halo} = 5.30 Å) and the π–π reflection ($d_{\pi-\pi}$ = 3.53 Å) (Fig. S48 and Table S3). As discussed above, the small-angle reflections were assigned as (10), (11), and (20) reflections of a Col_{ho} phase (*p6mm*) with a lattice parameter a = 29.0 Å.[40,42,43] Interestingly, when temperature-dependent XRD experiments were carried out (Table S4 and Fig. S48c, d), the intensity of the (10) reflection decreased with decreasing temperature and disappeared below 69 °C, whereas the (11), (20) reflections and the two diffuse wide-angle reflections remained. Such behavior was rather unexpected for Col_{ho}. However, it should be noted that Donnio and co-workers reported that ionic mesogens having a Col_{ho} mesophase had a missing (10) reflection when large, perfluorinated anions were used.[45] Presumably, the molecular form factor in **BON-LC3-F** was reduced and finally disappeared.

Mesomorphic properties of mixtures

We next explored mixtures of materials containing 1 wt% of emitter **BON-LC3-F**. Under POM, the mixture **LC3-F : BON-LC3-F** (99 : 1, w/w) displayed shearable textures with homeotropic areas and line defects, which are characteristic for the host **LC3-F** (Fig. S49).[37–39] The mixture **LC7-F : BON-LC3-F** (99 : 1, w/w) containing the larger host **LC7-F** also showed homeotropic areas with line defects as well as fan-shaped textures upon

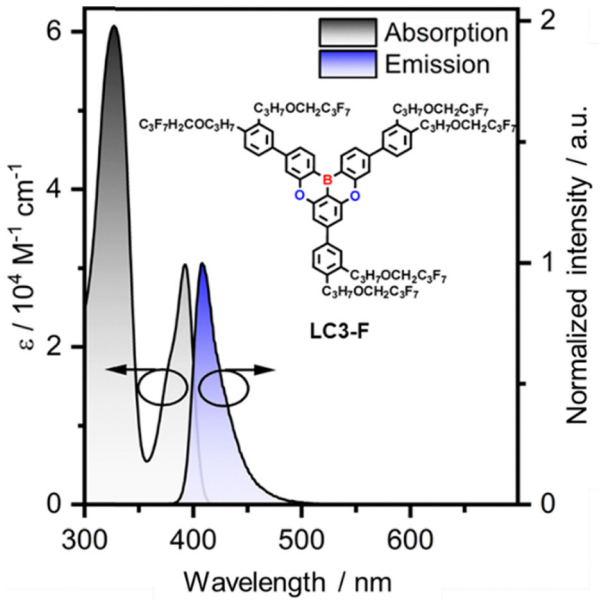

Fig. 4 Steady-state absorption (black trace) and emission (blue trace) spectra of **LC3-F** in degassed toluene (c = 0.02 mM, λ_{exc} = 320 nm).

heating (or cooling) (Fig. S50). Both mixtures displayed distinct phase transitions without phase separation.

Investigation of the mixture **LC3-F : BON-LC3-F** (99 : 1, w/w) by DSC revealed that upon 2nd cooling, there were clearing and glass transitions at 176.1 and −52.9 °C, respectively (Fig. 2b and Table S2). Both transition temperatures are higher as compared to those of **LC3-F** (Fig. 2c). The phase width (ΔT = 229 K) of the mixture is slightly smaller than the phase widths of the host **LC3-F**. The mixture **LC7-F : BON-LC3-F** (99 : 1, w/w) possesses a higher clearing temperature (237.2 °C) and a somewhat lower glass transition (−60.8 °C) (Fig. S51 and Table S2) resulting in a phase width (ΔT = 298 K), which that is identical with the temperature range of **LC7-F** yet much larger than for the mixture **LC3-F : BON-LC3-F** (99 : 1, w/w).

The 2D WAXS pattern of an oriented fiber showed orthogonal wide- and small-angle reflections for **LC3-F** doped with 1 wt% **BON-LC3-F** (Fig. 3c and Table S3). The two broad reflections in the wide-angle region were fitted by Lorentz functions, which provided d_{halo} = 4.51 Å and $d_{\pi-\pi}$ = 3.47 Å. In the SAXS, characteristic (10), (11), (20), and (21) reflections of a Col_{ho} phase ($p6mm$) with a lattice parameter of a = 32.1 Å were detected.[46–48] Thus, the mixture **LC3-F : BON-LC3-F** (99 : 1, w/w) possesses very similar mesophase geometries as compared to the pure host **LC3-F** (Fig. S52 and Table S3). The mixture **LC7-F : BON-LC3-F** (99 : 1, w/w) also showed a Col_{ho} phase ($p6mm$) (Fig. S53 and Table S3). Again, the lattice parameter of the mixture and the pure host **LC7-F** were identical (a = 40.5 Å). These results indicate that the mesomorphism of the host remains almost untouched by the guest.

Photophysical properties of LC3-F and LC7-F

The absorption spectrum of host **LC3-F** in toluene displays two intense bands at λ_{abs} = 327 nm (ε = 3.9 × 104 M^{-1} cm^{-1}) and 391 nm (ε = 3.1 × 104 M^{-1} cm^{-1}) (Fig. 4 and Table S5). The low-energy band was assigned to the SRCT transition of the substituted DOBNA core and is situated similarly to those of **DOBNA-Ph** (λ_{abs} = 395 nm)[34] and **LC8** (λ_{abs} = 393 nm),[26] but red-shifted as compared to **DOBNA** (λ_{abs} = 376 nm).[34] The high-energy band was assigned to a locally excited state of the mesogenic groups of **LC3-F**, which was also found in **LC8** (λ_{abs} = 340 nm) and **DOBNA-Ph** (λ_{abs} = 320 nm), but is absent in **DOBNA**. Upon excitation of **LC3-F** at 330 nm in degassed toluene, a deep blue narrowband emission at λ_{PL} = 408 nm (full-width at half maximum, FWHM = 26 nm) was observed. The Stokes shift is small (18 nm), reflecting the small degree of structural reorganization in the excited state. The Φ_{PL} is 56% (Table 1 and Table S5).[49–51] The PL band is nearly identical to that of **LC8** (λ_{PL} = 408 nm, Φ_{PL} = 63%),[26] and **DOBNA-Ph** (λ_{PL} = 410 nm, Φ_{PL} = 60%),[34] and is red-shifted compared to that of **DOBNA** (λ_{PL} = 398 nm, Φ_{PL} = 72%). Time-resolved PL

Table 1 Photophysics of hosts, emitter and host–emitter mixtures

Compound	Conditions	λ_{PL}/nm	FWHM/nm (FWHM/eV)	Φ_{PL}/%	$\tau_{p,avg}$/ns	τ_d/μs
LC8	Toluene	408	24 (0.18)	63	3.65	n.d.[a]
LC3-F	Toluene	408	26 (0.19)	56	4.47	n.d.[a]
LC7-F	Toluene	408	27 (0.20)	59	4.14	n.d.[a]
BON-LC12	Toluene	466	23 (0.13)	77	6.75	n.d.[a]
BON-LC3-F	Toluene	461	23 (0.13)	76	5.85	n.d.[a]
LC8	Neat	472	70 (0.40)	19	16.62	n.d.[a]
LC3-F	Neat	460	63 (0.36)	19	15.42	n.d.[a]
LC7-F	Neat	457	59 (0.34)	20	13.29	n.d.[a]
BON-LC12	Neat	544	77 (0.33)	39	31.96	n.d.[a]
BON-LC3-F	Neat	528	72 (0.31)	30	30.18	35.0
LC8[c]	PS	476	14 (0.08)	41	8.19	n.d.[a]
BON-LC12[d]	PS	467	45 (0.25)	90	9.85	107.8
BON-LC3-F[e]	PS	463	65 (0.35)	n.d.[b]	5.37	142.6
BON-LC3-F:LC3-F[f]	PS	477	41 (0.22)	54	15.20	52.05
BON-LC3-F:LC7-F[f]	PS	478	43 (0.23)	49	16.99	56.1

[a] No delayed emission observed. [b] The quantum yield could not be determined due to the low absorption of the film. [c] **LC8** in doped (1 wt% BCzBN) polystyrene (PS) films. [d] **BON-LC12** in PS film (1 wt%). [e] **BON-LC3-F** in PS film (0.1 wt%). [f] **BON-LC3-F** in a PS film in **LC3-F** (1 wt%) or **LC7-F** (1 wt%).

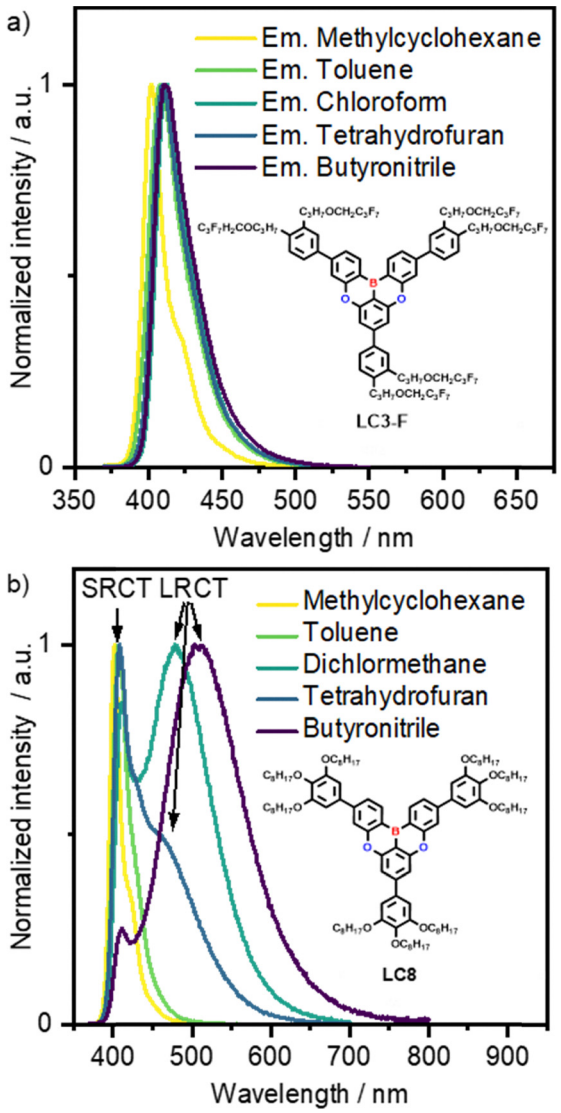

Fig. 5 (a) Solvatofluorochromism of **LC3-F** in different solvents (c = 0.01 mM, λ_{exc} = 330 nm); (b) solvatofluorochromism of **LC8** in different solvents (c = 0.02 mM, λ_{exc} = 350 nm).

measurements revealed monoexponential decay kinetics, with a τ_p = 4.47 ns (Fig. S54b and Table S5), which is slightly slower than for **LC8** (τ_p = 3.65 ns) and for **DOBNA-Ph** (τ_p = 5.61 ns) and **DOBNA** (τ_p = 1.07 ns). The photophysical properties of **LC3-F** are similar to the alkoxy analogue **LC8**.[26]

Solvent-dependent steady-state absorption and PL measurements revealed that there is effectively no change in the absorption spectrum with solvent polarity, reflecting the non-polar ground state of **LC3-F** (Fig. S54c and Table S6), while there is a small bathochromic shift from λ_{PL} = 402 nm (MCH) to 410 nm (butyronitrile) that is characteristic of an excited state of SRCT character (Fig. 5a). In comparison with the PL spectrum of **LC8** (Fig. 5b), there is no low-lying LRCT state that becomes stabilized in polar media, and the emissive SRCT excited state is retained across all of these solvents in **LC3-F**.

Next, we determined the S_1 and T_1 levels of **LC3-F** from the onsets of the steady-state PL and phosphorescence spectra in frozen 2-MeTHF glass at 77 K (Fig. S54e). The obtained energies (S_1 = 3.12 eV, T_1 = 2.79 eV) result in a ΔE_{ST} of 0.32 eV (Table S5).[49] Compared to **LC8**, the T_1 state of **LC3-F** is destabilized by 0.09 eV. Moreover, comparison of the S_1 and T_1 levels (determined from the maxima) of **LC3-F** (S_1 = 3.05 eV, T_1 = 2.68 eV) with alkoxy derivative **LC8** (T_1 = 2.41 eV) and **DOBNA-Ph** (T_1 = 2.71 eV, EtOH, 77 K) clearly indicated that the T_1 level of **LC3-F** is only destabilized by 0.03 eV compared to **DOBNA-Ph**, whereas **LC8** is destabilized by 0.29 eV. The derivative **LC7-F** has very similar photophysical properties in degassed toluene solution (λ_{PL} = 408 nm, FWHM = 27 nm, Φ_{PL} = 59%) and identical S_1 and T_1 levels to those of **LC3-F** (Table 1, Fig. S55, Table S5). Thus, the nature of the chain exerts no influence on the photophysical properties, in agreement with the previous observations made for the DOBNA alkoxy series **LCn**.[26] The solution studies demonstrated that monomolecular species of **LC3-F** and **LC7-F** maintain the SRCT character of the S_1 state in contrast to derivatives carrying alkoxy side chains, where the S_2 state of LRCT character is stabilized. Further, **LC3-F** and **LC7-F** possess higher T_1 levels, thus increasing their suitability as host materials for blue emitters.

Next, the photophysical properties of the bulk phase of **LC3-F**, **LC7-F** were examined to determine whether the observed trends in solutions of **LC3-F**, **LC7-F** are also maintained in the bulk LC phase in the presence of columnar aggregates in thin films. It should be noted that thin films of **LC3-F** and **LC7-F** were prepared by drop-casting $CHCl_3$ solutions rather than spin-coating because the latter method did not produce stable films, presumably due to the fluorophobic effect of the side chains with the quartz and sapphire substrates. The absorption spectrum of the thin film of **LC3-F** showed two bands at λ_{abs} = 330 and 396 nm, respectively (Table S5, entry 4), which are blue-shifted by 5 and 4 nm compared to the solution spectrum (Table S5, entry 1). Despite the strong aggregation in the Col_{ho} phase, very little electronic interaction in the ground state was found.[52,53] Compared to the solution-state PL spectrum, that in the solid state is bathochromically shifted and broadened (λ_{PL} = 460 nm, FWHM = 63 nm, Fig. 6a and Table 1). This implies excimer emission.[20,27,54] Compared to the Φ_{PL} in solution, the value of the film is much lower at 19%, presumably due to significant ACQ.[54] The results are in good agreement with those observed for **LC8**.[26]

Time-resolved PL measurements of **LC3-F** by TCSPC (Fig. S57b and Table S8) showed a triexponential decay of the PL emission, with an average prompt lifetime $\tau_{p,avg}$ = 15.42 ns (Table 1) that is slightly shorter than that of **LC8** ($\tau_{p,avg}$ = 16.62 ns).[26] Excited-state levels of **LC3-F** in the bulk (S_1 = 2.94 eV, T_1 = 2.62 eV) are stabilized by 0.18 and 0.17 eV, respectively, as compared to the energy levels in solution, reflecting the state energies of the excimer. Unfortunately, the resulting ΔE_{ST} of 0.32 eV is large and thus no delayed emission was detected. In comparison to **LC8**, the T_1 level of **LC3-F** in the bulk is destabilized by 0.05 eV. The photophysical properties of the homologous derivative **LC7-F** (λ_{PL} = 457 nm, FWHM = 59 nm, Φ_{PL} = 20%, Table 1 and Fig. S58) also reflect excimer

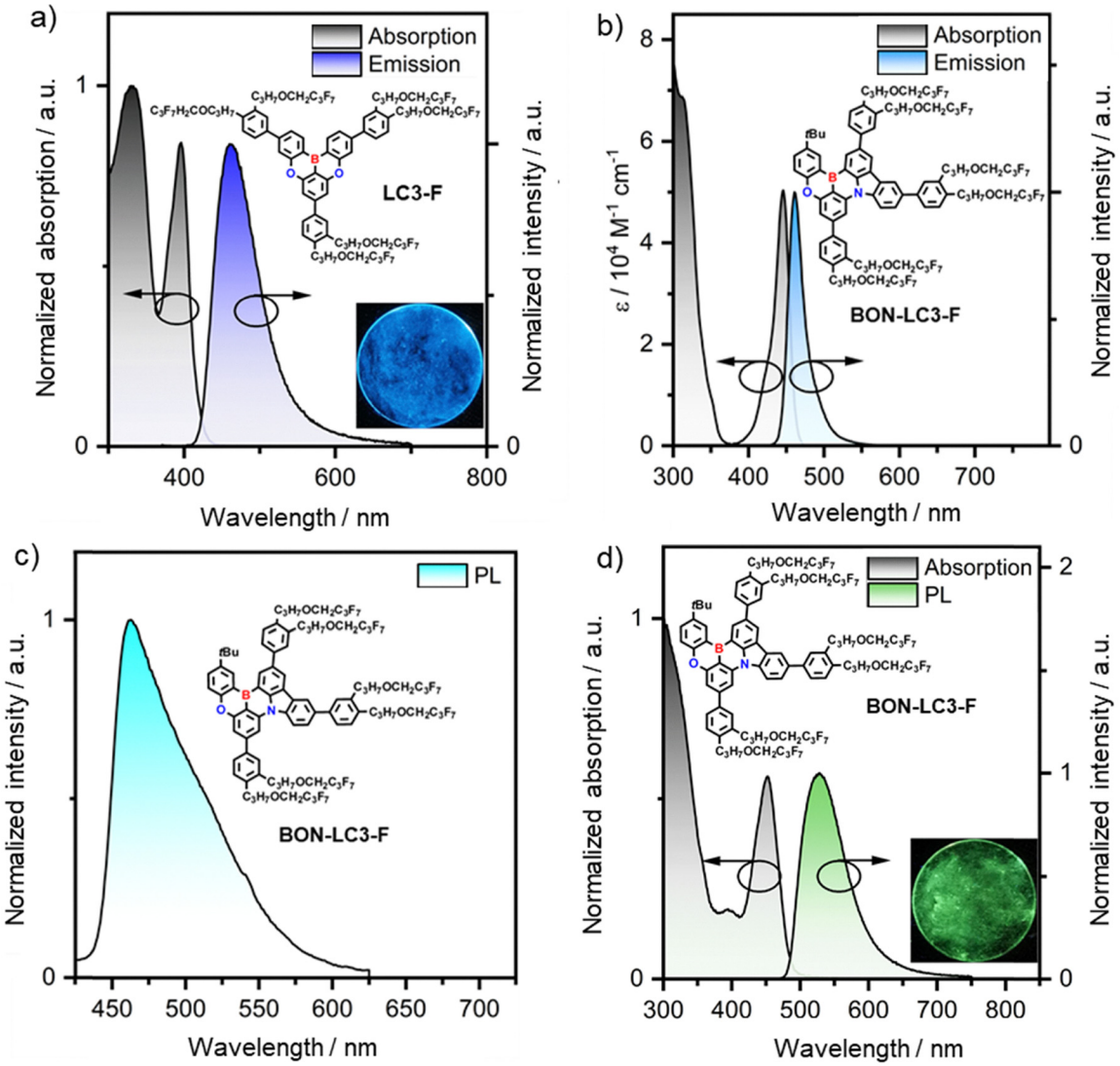

Fig. 6 (a) Absorption (black trace) and steady-state emission (blue trace, λ_{exc} = 320 nm) of **LC3-F** in a neat film, inset shows the film under UV light; (b) steady-state absorption (black trace) and emission (blue trace) (λ_{exc} = 410 nm) spectra of **BON-LC3-F** in degassed toluene; (c) photoluminescence spectrum of **BON-LC3-F** in polystyrene; (d) absorption (black trace) and steady-state emission (blue trace, λ_{exc} = 440 nm) of **BON-LC3-F** in a neat film, the inset shows the film under UV light.

formation in the Col_{ho} phase.[20,27,54] The T_1 level of **LC7-F** is destabilized by 0.11 eV as compared to that of **LC8**. Thus, the thin film studies with **LC3-F** and **LC7-F** revealed a higher energy T_1 level in the bulk Col_{ho} phase (T_1 = 2.62 and 2.65 eV, respectively), indicating that **LC3-F** and **LC7-F** are suitable host materials for the MR-TADF emitter **BON-LC3-F** (T_1 = 2.51 eV) in contrast to their **LCn** DOBNA counterparts, which contain alkoxy chains.

Photophysical properties of BON-LC3-F

In dilute toluene solution, **BON-LC3-F** exhibits a strong absorption at λ_{abs} = 446 nm and a sharp sky-blue PL emission at λ_{PL} = 461 nm (FWHM = 23 nm) associated with a Φ_{PL} of 76% (Table 1, Fig. S56, Table S5).[49–51] Comparison to the parent **B-OCz** emitter[55] revealed that both the absorption and emission maxima are red-shifted, by 21 and 20 nm, respectively. Time-resolved PL measurements in degassed toluene showed a $\tau_{p,avg}$ of 5.86 ns (Fig. S56b). Comparison to **BON-LC** showed that the emission is slightly blue-shifted (λ_{PL} = 466 nm, FWHM = 23 nm, Φ_{PL} = 77%),[23] but otherwise this compound shows very similar behavior.

Solvatochromism measurements support the assignment of the SRCT character to the emissive excited state (Fig. S56c, d and Table S6). To investigate whether **BON-LC3-F** is a suitable MR-TADF emitter, S_1 and T_1 energies were determined from the onsets of the steady-state PL and phosphorescence spectra in frozen 2-MeTHF glass at 77 K (S_1 = 2.75 eV, T_1 = 2.57 eV) (Fig. S56e). Thus, the ΔE_{ST} is 0.18 eV (Table S5), which is 0.11 eV larger than that for **BON-LC12** (ΔE_{ST} = 0.07 eV).[23,56,57] These results suggest that **BON-LC3-F** can act as a suitable dopant

with the hosts **LC3-F** and **LC7-F**. No delayed fluorescence was detected for **BON-LC3-F** in solution, similar to many reported MR-TADF emitters that do not show delayed emission in solution, presumably due to competing non-radiative decay.[18,23,26] Therefore, a doped film of **BON-LC3-F** in polystyrene (PS, 0.1 wt%) was studied. In this matrix, there is an intense PL signal at λ_{PL} = 463 nm that is significantly broadened (FWHM = 65 nm, Fig. S60a), presumably caused the strong tendency of the dye molecules to aggregate (Fig. 6c and Table 1). From the energy levels (S_1 = 2.82 eV, T_1 = 2.58 eV), a slightly larger ΔE_{ST} of 0.24 eV was determined, due to the S_1 level being destabilized (Fig. S60c and Table S5). Prompt lifetime measurements by TCSPC showed a triexponential decay with $\tau_{p,avg}$ = 5.37 ns, while MCS TR PL measurements revealed delayed emission with a lifetime of τ_d = 142.6 µs, which was completely quenched by oxygen (Table 1 and Fig. S62b, d). Temperature-dependent time-resolved PL measurements by MCS indicated that the magnitude of the delayed emission increases with increasing temperature, a hallmark of TADF behavior (Fig. S60e). Thus, **BON-LC3-F** is an MR-TADF emitter.[58–60]

In comparison with **BON-LC12**, the PL band of **BON-LC3-F** is broadened due to the increased tendency of the semiperfluorinated derivative towards aggregation. The delayed lifetime of **BON-LC3-F** (τ_d = 142.6 µs) is significantly longer than for **BON-LC12** (τ_d = 107.8 µs), reflecting its larger ΔE_{ST}.[23] These results demonstrate that the photophysical properties of the MR-TADF emitter are maintained in the presence of the semiperfluorinated side chains.

Drop-cast thin films of **BON-LC3-F** showed an absorption band at λ_{abs} = 452 nm (Fig. 6d and Table 1), which is slightly bathochromically shifted and somewhat broadened compared to that in toluene, which indicates that there are only few intermolecular interactions in the ground state despite the strongly aggregated Col_{ho} mesophase.[52,53] In contrast to the sky-blue emission in toluene (λ_{PL} = 461 nm) or PS (λ_{PL} = 463 nm), a green emission (λ_{PL} = 528 nm) was observed in the neat film (Fig. 6d and Table S5). The large Stokes shift

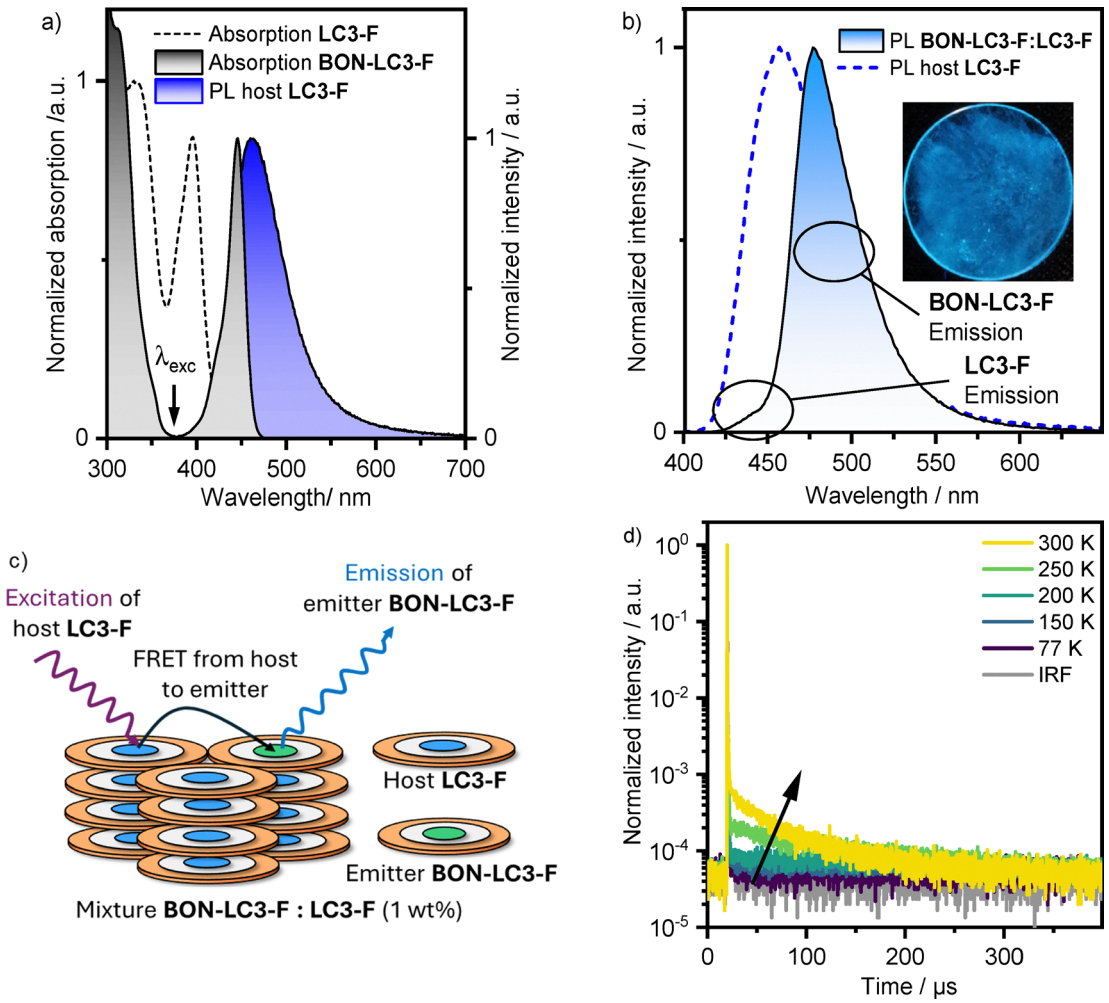

Fig. 7 (a) Comparison of the absorption spectra of the host material **LC3-F** (dashed line) and the emitter **BON-LC3-F** (in toluene, c = 0.02 mM, black) with the emission spectrum of neat **LC3-F** (λ_{exc} = 350 nm, blue); (b) PL-spectrum of a **LC3-F** : **BON-LC3-F** (99 : 1, w/w) blend (λ_{exc} = 375 nm, light blue) compared to that of the pure host **LC3-F** (λ_{exc} = 350 nm, blue dashed line), the inset shows the film under UV light; (c) possible Förster resonance energy transfer (FRET) from the host **LC3-F** to the emitter **BON-LC3-F**; (d) temperature-dependent MCS-lifetime measurements.

(82 nm), the significant PL broadening (FWHM = 72 nm), and the much reduced Φ_{PL} of 30% compared to the data acquired in toluene solution all point to excimer emission. This is similar behavior to that observed for the neat film photophysics of other MR-TADF emitters.[20,27,54] Time-resolved PL measurements by TSCPC reveal a triexponential decay with a $\tau_{p,avg}$ = 30.18 ns (Fig. S59b and Table S7). The ΔE_{ST} is reduced to 0.08 eV, and the τ_d is 35 µs (Table S5). Not surprisingly, the PL is sensitive to O_2, the temperature-dependent time-resolved PL measurements also document TADF behavior (Fig. S59d and Table S5). Above 300 K, both the intensity of the delayed lifetime as well as the PL intensity decrease, which reflects increased temperature-dependent non-radiative decay that may originate from increased vibrational relaxation in the mesophase (T_g = 256 K) of **BON-LC3-F**.[61] In comparison with **BON-LC12** (λ_{PL} = 544 nm, FWHM = 77 nm, Φ_{PL} = 39%), **BON-LC3-F** showed similar photophysical properties as a neat film, with a small observed blue-shift of the PL maximum. Thus, in both molecules, the photophysical properties of the neat film reflect excimer formation in the strongly aggregated Col_{ho} phase. Despite these similarities, it should be emphasized that a neat film of **BON-LC12** does not show TADF, while that of **BON-LC3-F** does.

Photophysical properties of the host–emitter mixtures

A qualitative comparison of the absorption spectra of the host **LC3-F** in the bulk state and the absorption of the emitter **BON-LC3-F** in toluene (Table 1) revealed that at the chosen excitation wavelengths λ_{exc} = 379 nm, only the host **LC3-F** should absorb and thus a direct excitation of the emitter does not take place (Fig. 7a).[62] Moreover, the PL band of the host **LC3-F** and the absorption band of the emitter **BON-LC3-F** show sufficient overlap to permit an efficient energy transfer from host to emitter.[63] The film of the mixture **LC3-F:BON-LC3-F** (containing 1 wt% of the emitter **BON-LC3-F**) displays a sky blue emission (λ_{PL} = 477 nm, FWHM = 41 nm, Φ_{PL} = 54%, Fig. 7b

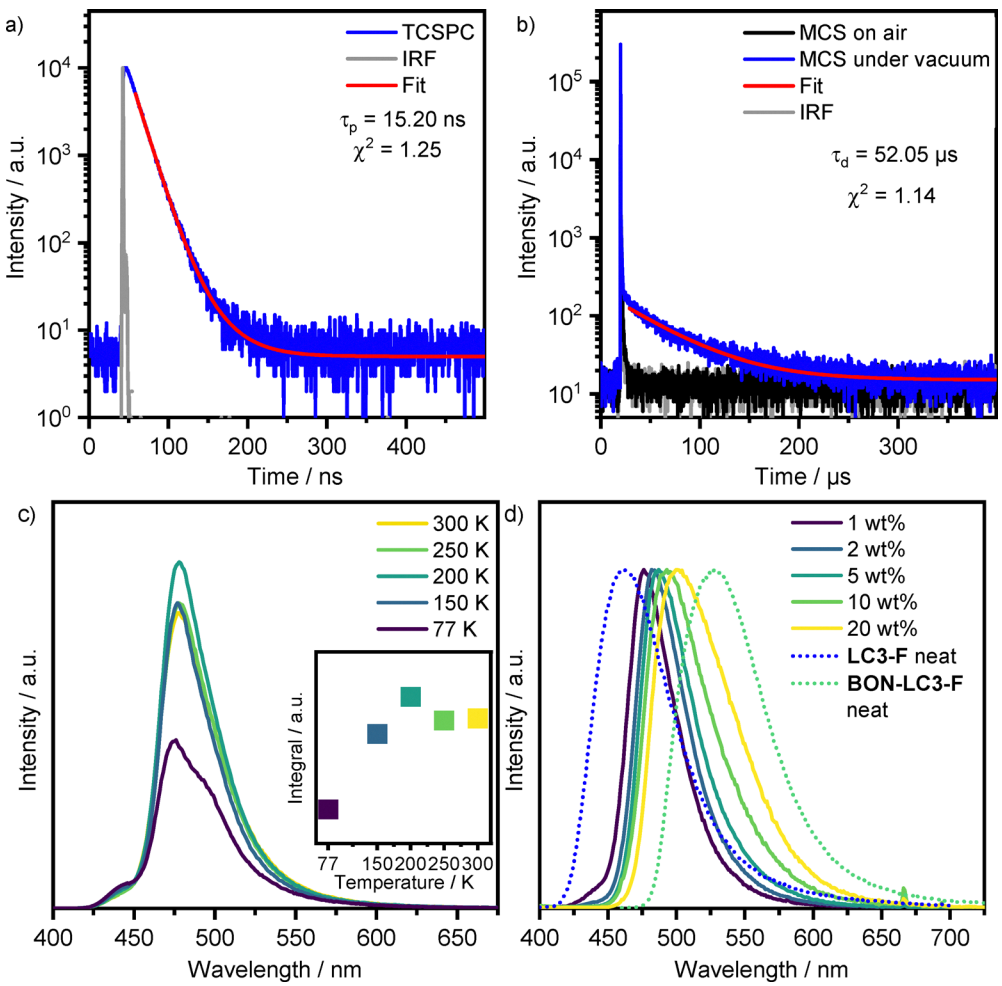

Fig. 8 Photophysical properties of the **BON-LC3-F** : **LC3-F** (99 : 1, w/w) blend (λ_{exc} = 375 nm; for TCSPC and MCS measurements: λ_{exc} = 379 nm): (a) time-correlated single photon counting (TCSPC) lifetime measurement (blue curve) with a triple-exponential decay fit (red curve) and instrument response function (IRF, grey); (b) microsecond-scale time-resolved emission (MCS) lifetime measurement in air (black curve) and under vacuum (blue curve) with a mono-exponential decay fit (red curve) and IRF (grey); (c) temperature-dependent PL-spectra, the inset shows the integrated intensity of the **BON-LC3-F** emission band (integration range: 450–650 nm); (d) steady state emission of **BON-LC3-F** (1, 2, 5, 10, 20 wt%) doped into **LC3-F**. Steady-state emission of neat **BON-LC3-F** (green dashed trace) and neat **LC3-F** (blue dashed traces) is given for comparison.

and Table 1), which was assigned to the emission of **BON-LC3-F**. In addition, the emission spectrum of the mixture shows a small shoulder at λ_{PL} = 450 nm, which was assigned to emission from the host **LC3-F**. It should be noted that there is no excimer emission at λ_{PL} = 530 nm resulting from aggregation of the emitter **BON-LC3-F**. Presumably, the emitter is well integrated in the liquid crystalline matrix of the host, which effectively suppresses emitter aggregation. In comparison to the PL spectrum of **BON-LC3-F** in toluene (λ_{PL} = 461 nm, FWHM = 23 nm), the PL band of the mixture is bathochromically shifted by 16 nm and somewhat broadened, indicating weak interactions between host and emitter, as well as emitter/emitter interactions, in the mixture.[64,65] Thus, in the mixture, there is almost complete energy transfer from the host **LC3-F** to the emitter **BON-LC3-F**. Based on the significantly increased Φ_{PL} of the mixture to 54% as compared to the host **LC3-F** (Φ_{PL} = 19%), the energy transfer occurs almost certainly *via* FRET.[62,63,66–68]

From the PL and phosphorescence spectra of the mixture at 77 K, the energy levels S_1 = 2.74 eV and T_1 = 2.60 eV were extracted. The ΔE_{ST} of the mixture of 0.14 eV is similar to the ΔE_{ST} value of the emitter **BON-LC-F$_3$** (ΔE_{ST} = 0.18 eV in toluene) and significantly different from that of the neat host **LC3-F** (ΔE_{ST} = 0.32 eV in the bulk), further supporting the assignment of the PL bands (for details, see Table S5). Lifetime measurements showed a biexponential decay of the prompt fluorescence ($\tau_{p,avg}$ = 15.20 ns) and a delayed fluorescence with single exponential decay (τ_d = 52.05 μs), which was quenched by O_2 (Fig. 8a and b). Temperature-dependent time-resolved PL measurements confirm that the mixture exhibits TADF[58–60] (Fig. 8c).[61,69–71] Upon increasing the emitter concentration in the host **LC3-F** (Fig. 8d and Table S8), the PL bands bathochromically shifted and broadened from λ_{PL} = 477 nm, FWHM = 41 nm (1 wt%) to λ_{PL} = 501 nm, FWHM = 68 nm (20 wt%), resulting from the increased intermolecular emitter–emitter interactions in the columnar mesophase of the mixture (for further details, see Fig. S62).

The analogous mixture **LC7-F : BON-LC3-F** (99 : 1, w/w) shows very similar photophysical behavior, with a distinct PL band from the emitter at λ_{PL} = 478 nm (FWHM = 43 nm, Φ_{PL} = 49%, τ_d = 56.1 μs) (Table 1 and Fig. S62). Thus, the excitation energy is likewise transferred *via* FRET from the host **LC7-F** to the emitter **BON-LC3-F**.

Packing model of the mixtures

We surmised that the observed photophysical and mesomorphic properties may be rationalized by a distinct packing model of the mesophase. In principle, for binary mixtures of columnar liquid crystals with similar molecular scaffolds and lattice parameters, three different packing geometries are possible (Fig. 9a). The first is one where host and emitter molecules may undergo a macroscopic phase separation similar to the arrangement of block copolymers,[72,73] if host and emitter are non-miscible. The second is one where the host and emitter are partially miscible and intercolumnar phase separation may occur, *i.e.*, columns of host are mixed with columns of emitter, resulting in intercolumnar mixed phases.[20,72,73] Finally, if host

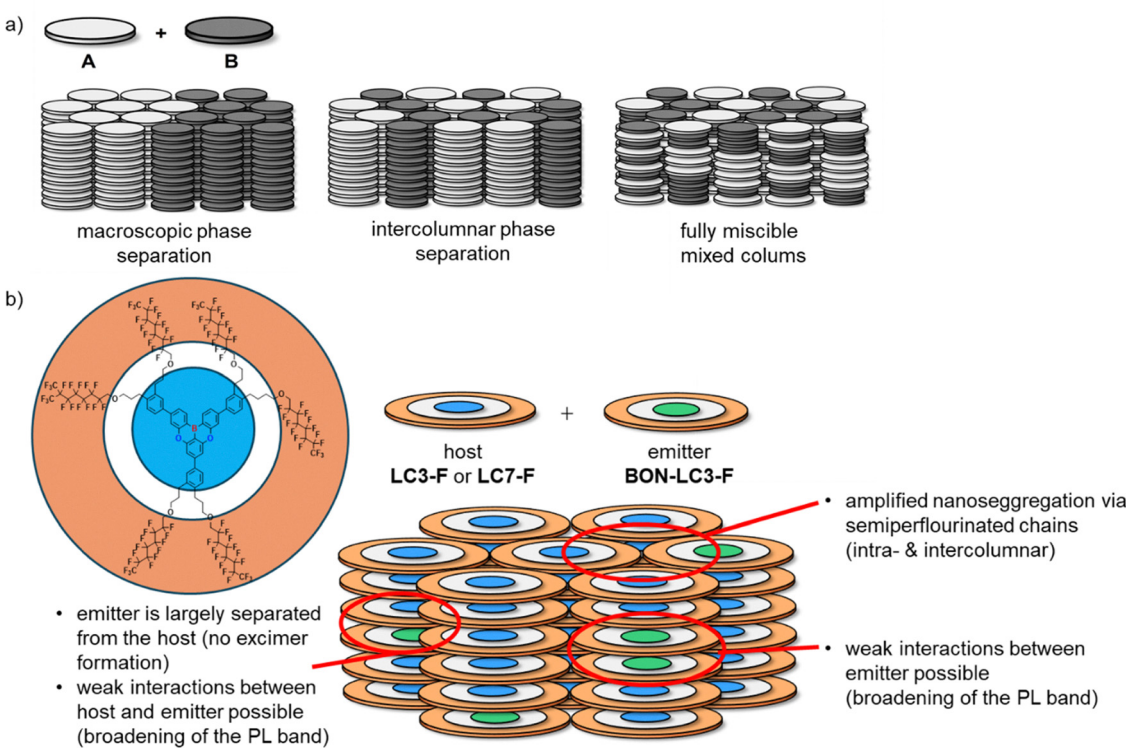

Fig. 9 (a) Possible arrangements for binary mixtures of two columnar liquid crystals, A and B; (b) proposed packing model of the mixtures **BON-LC3-F : LC3-F** (99 : 1, w/w) and **BON-LC3-F : LC7-F** (99 : 1, w/w) based on X-ray diffraction data and the photophysical properties of the mixtures.

and emitter are fully miscible, each column contains mixtures of host and emitter, either in an alternating manner or blockwise separated.[20,74] Because the mixtures contain only 1 wt% of the emitter **BON-LC3-F**, the lattice parameters of the mixtures **LC3-F**: **BON-LC3-F** and **LC7-F**:**BON-LC3-F** are mostly governed by the host **LC3-F** or **LC7-F**. That there is the absence of any host excimer emission in the mixture implies that the first two packing models are highly unlikely and strongly supports a mixed columns model (Fig. 9b). The relatively broad PL bands of **BON-LC3-F** in these mixtures can be rationalized by weak interactions between emitter **BON-LC3-F** and hosts **LC3-F** (or **LC7-F**) or weak interactions between two emitter molecules closely located within a column. It should be noted that the semiperfluoroalkyl side chains have two distinct functions: (i) they are ''electronically neutral'' compared to the strongly electron-donating alkoxy chains. The electronic isolation is caused by the alkyl subunit. Thus, the S_1 and T_1 states are only slightly affected, and the ΔE_{ST} of both hosts **LC3-F**, **LC7-F** and emitter **BON-LC3-F**, respectively, remain similar to the parent non-mesogenic dyes **DOBNA** and **B-O-Cz**, respectively, whereas the ΔE_{ST} values for **LC8** and **BON-LC12** increased (Table S7). (ii) The semiperfluoroalkyl chains strengthen nanoseggregation through the perfluorinated subunit. This results in increased mesophase stabilities and temperature ranges for both neat films of these compounds as well as mixtures containing semiperfluorinated side chains rather than alkoxy chains (see Fig. 2c).

Conclusion

The first room-temperature columnar MR-TADF host–guest system is reported. This is based on a columnar DOBNA-derived host **LC3-F** (or **LC7-F**), and a columnar emitter **BON-LC3-F**. Semiperfluorinated side chains decorating both host and emitter improved nanosegregation and stabilized the columnar mesophases as compared to the corresponding host and emitter with alkoxy side chains. Temperature ranges of the columnar mesophase increased by 69 K for **LC3-F**, 193 K for **LC7-F**, and 238 K for **BON-LC3-F** as compared to the counterparts **LC8** and **BON-LC12** that contain alkoxy side chains. In the mixtures, no phase separation was observed by POM, and almost identical XRD data of neat hosts and host emitter mixtures revealed that the emitter **BON-LC3-F** blends perfectly into the host **LC3-F** (or **LC7-F**) mesophase.

Moreover, the semiperfluorinated side chains gratifyingly do not stabilize the excited states of the host, resulting in higher T_1 levels and smaller ΔE_{ST} as compared to analogous hosts carrying alkoxy side chains. Whereas the neat host **LC3-F** (or **LC7-F**) showed no TADF and the neat emitter **BON-LC3-F** showed only very weak TADF, mixtures **LC3-F : BON-LC3-F** (99 : 1, w/w) and **LC7-F : BON-LC3-F** (99 : 1, w/w) showed MR-TADF, with delayed lifetimes of τ_d = 52.0 μs and τ_d = 56.1 μs, respectively, due to energy transfer from host to emitter *via* FRET. Despite the large excess of the host material in the mixture (99 wt%), the PL bands of the mixtures originate from the 1 wt% of emitter. Consequently, with increasing relative amount of emitter, the Φ_{PL} increases from 54% (1 wt%) to 68% (5 wt%). The perfect integration of the emitter in the host was also deduced from the fact that no excimer emission of the emitter **BON-LC3-F** was detected in these mixtures.

Such ''turn-on'' TADF by mixing columnar hosts with columnar emitters provides a versatile approach by choosing suitable combinations of host (determining the LC properties) and emitter (determining the photophysical properties), while ACQ of columnar self-assembled dye molecules was overcome by high dilution of the emitter in the host. Such approach should be amenable to other compound classes of host and emitter useful for various optoelectronic applications. Future work must demonstrate whether the beneficial effect of fluorophobic self-assembly reported for organic transistors is also true for OLED devices.

Author contributions

J. A. K. conceived and supervised the project and performed the synthesis as well as characterization. T. G. performed part of the synthesis. T. M. helped with characterization, computation and manuscript preparation. S. L. and A. Z. wrote the manuscript. A. Z. checked the data. E. Z.-C. and S. L. supervised the project and the manuscript preparation.

Conflicts of interest

There are no conflicts of interest.

Data availability

Additional raw data files are available from the corresponding author upon reasonable request. The research data supporting this publication can be accessed at https://doi.org/10.17630/45e47c51-fa07-455e-98d5-22f2328a37ba.

The data supporting the findings of this study are available within the article and its supplementary information (SI). Supplementary information: ^{1}H NMR and ^{13}C NMR spectra, HRMS, and GPC traces; details of X-ray crystallography, DSC, and POM; supplemental photophysical data. See DOI: https://doi.org/10.1039/d5tc03809j.

Acknowledgements

Generous financial support by the Studienstiftung des deutschen Volkes (PhD fellowship for J. A. K.), the Ministerium für Wissenschaft, Forschung und Kunst des Landes Baden Württemberg, the Carl Schneider Stiftung Aalen (shared instrumentation grant), the Universität Stuttgart (Global glimpse travel grant for J. A. K.) and the DFG (INST 41/897-1 FUGG for 700 MHz-NMR, INST 41/1136-1 FUGG for LC-Orbitrap-MS: Exactive Plus Orbitrap MS System and INST 41/1135-1 FUGG for GC-Orbitrap-MS: Exactive GC Orbitrap MS System) are gratefully acknowledged. The St Andrews team would also like to thank

EPSRC (EP/Z535291/1, EP/W007517/1, and EP/W015137/1) for financial support.

Notes and references

1 M. E. Prevot, J. P. Vanegas and E. Hegmann, Emissive Nanomaterials and Liquid Crystals, in *21st Century Nanoscience – A Handbook*, CRC Press, Boca Raton, 2020.
2 A. Kumar and G. Singh, *J. Mol. Liq.*, 2023, **386**, 122607.
3 Y. Wang, J. Shi, J. Chen, W. Zhu and E. Baranoff, *J. Mater. Chem. C*, 2015, **3**, 7993–8005.
4 A. Surampudi, G. Zhang, R. Singh, G. Faulkner, D. C. O'Brien, M. J. Booth and S. M. Morris, *Crystals*, 2023, **13**, 1615.
5 J. Uchida, B. Soberats, M. Gupta and T. Kato, *Adv. Mater.*, 2022, **34**, 2270171.
6 T. Wöhrle, I. Wurzbach, J. Kirres, A. Kostidou, N. Kapernaum, J. Litterscheidt, J. C. Haenle, P. Staffeld, A. Baro and F. Giesselmann, *Chem. Rev.*, 2016, **116**, 1139–1241.
7 S. Laschat, A. Baro, N. Steinke, F. Giesselmann, C. Hägele, G. Scalia, R. Judele, E. Kapatsina, S. Sauer and A. Schreivogel, *Angew. Chem., Int. Ed.*, 2007, **46**, 4832–4887.
8 R. De and S. K. Pal, *Chem. Commun.*, 2023, **59**, 3050–3066.
9 S. Sergeyev, W. Pisula and Y. H. Geerts, *Chem. Soc. Rev.*, 2007, **36**, 1902–1929.
10 R. K. Gupta and A. A. Sudhakar, *Langmuir*, 2018, **35**, 2455–2479.
11 Y. Zhu, S. Zeng, B. Li, A. J. McEllin, J. Liao, Z. Fang, C. Xiao, D. W. Bruce, W. Zhu and Y. Wang, *ACS Appl. Mater. Interfaces*, 2022, **14**, 15437–15447.
12 A. F. Suleymanova, M. Z. Shafikov, A. C. Whitwood, R. Czerwieniec and D. W. Bruce, *J. Mater. Chem. C*, 2021, **9**, 6528–6535.
13 A. F. Suleymanova and M. Z. Sha, *Phys. Chem. Chem. Phys.*, 2022, **24**, 22115–22121.
14 D. Chen, F. Tenopala-Carmona, J. A. Knöller, A. Mischok, D. Hall, S. Madayanad Suresh, T. Matulaitis, Y. Olivier, P. Nacke and F. Gießelmann, *Angew. Chem., Int. Ed.*, 2023, **62**, e202218911.
15 G. Schweicher, G. Gbabode, F. Quist, O. Debever, N. Dumont, S. Sergeyev and Y. H. Geerts, *Chem. Mater.*, 2009, **21**, 5867–5874.
16 R. I. Gearba, D. V. Anokhin, A. I. Bondar, W. Bras, M. Jahr, M. Lehmann and D. A. Ivanov, *Adv. Mater.*, 2007, **19**, 815–820.
17 B. He, Q. Zhong, Q. Dong, X. Yang, S. J. Cowling, W. Qiao, D. W. Bruce, W. Zhu, P. Duan and Y. Wang, *Mater. Horiz.*, 2024, **11**, 1251–1260.
18 J. M. Dos Santos, D. Hall, B. Basumatary, M. Bryden, D. Chen, P. Choudhary, T. Comerford, E. Crovini, A. Danos and J. De, *Chem. Rev.*, 2024, **124**, 13736–14110.
19 M. Y. Wong and E. Zysman-Colman, *Adv. Mater.*, 2017, **29**, 1605444.
20 B. Adelizzi, P. Chidchob, N. Tanaka, B. A. Lamers, S. C. Meskers, S. Ogi, A. R. Palmans, S. Yamaguchi and E. W. Meijer, *J. Am. Chem. Soc.*, 2020, **142**, 16681–16689.
21 A. F. Suleymanova, J. R. Fortwengler, X. Chen, R. Czerwieniec, Y. Wang, M. Z. Shafikov and D. W. Bruce, *J. Mater. Chem. C*, 2025, **13**, 12348–12364.
22 L. G. Franca, P. L. Dos Santos, P. Pander, M. G. Cabral, R. Cristiano, T. Cazati, A. P. Monkman, H. Bock and J. Eccher, *ACS Appl. Electron. Mater.*, 2022, **4**, 3486–3494.
23 J. A. Knöller, B. Sönmez, T. Matulaitis, A. K. Gupta, E. Zysman-Colman and S. Laschat, *Chem. Commun.*, 2024, **60**, 4459–4462.
24 N. Li, F. Ni, X. Lv, Z. Huang, X. Cao and C. Yang, *Adv. Opt. Mater.*, 2022, **10**, 2101343.
25 T. Chatterjee and K.-T. Wong, *Adv. Opt. Mater.*, 2019, **7**, 1800565.
26 J. A. Knöller, F. Müller, T. Matulaitis, J. M. Dos Santos, A. K. Gupta, E. Zysman-Colman and S. Laschat, *Chem. Sci.*, 2024, **15**, 18022–18030.
27 S. Xu, Q. Yang, Y. Zhang, H. Li, Q. Xue, G. Xie, M. Gu, J. Jin, L. Huang and R. Chen, *Chin. Chem. Lett.*, 2021, **32**, 1372–1376.
28 C. Tschierske, *Top. Curr. Chem.*, 2012, **318**, 1–108.
29 B. J. Jung, K. Lee, J. Sun, A. G. Andreou and H. E. Katz, *Adv. Funct. Mater.*, 2010, **20**, 2930–2944.
30 K. Miao, G. J. Chae, X. Wu, Q. Shu, X. Zhu, B. Sun, J. Fan and S. Cho, *RSC Adv.*, 2016, **6**, 29164–29171.
31 H.-G. Jeong, B. Lim, D. Khim, M. Han, J. Lee, J. Kim, J.-M. Yun, K. Cho, J.-W. Park and D.-Y. Kim, *Adv. Mater.*, 2013, **25**, 6416–6422.
32 J. C. Haenle, Y. Stöckl, R. Forschner, E. Haenle and S. Laschat, *ChemPhysChem*, 2018, **19**, 2758–2767.
33 P. Ehni, S. M. Bauch, P. M. Becker, W. Frey, A. Zens, J. Kästner, Y. Molard and S. Laschat, *Phys. Chem. Chem. Phys.*, 2022, **24**, 21617–21630.
34 H. Hirai, K. Nakajima, S. Nakatsuka, K. Shiren, J. Ni, S. Nomura, T. Ikuta and T. Hatakeyama, *Angew. Chem., Int. Ed.*, 2015, **54**, 13581–13585.
35 X. Cai, J. Xue, C. Li, B. Liang, A. Ying, Y. Tan, S. Gong and Y. Wang, *Angew. Chem., Int. Ed.*, 2022, **61**, e202200337.
36 T. Wang, X. Yin, X. Cao and Y. Yang, *Angew. Chem., Int. Ed.*, 2023, **62**, e202312451.
37 R. Forschner, J. Knelles, K. Bader, C. Müller, W. Frey, A. Köhn, Y. Molard, F. Giesselmann and S. Laschat, *Chem. – Eur. J.*, 2019, **25**, 12966–12980.
38 J. A. Lugger, D. J. Mulder, S. Bhattacharjee and R. P. Sijbesma, *ACS Nano*, 2018, **12**, 6714–6724.
39 G. Zucchi, B. Donnio and Y. H. Geerts, *Chem. Mater.*, 2005, **17**, 4273–4277.
40 U. Dahn, C. Erdelen, H. Ringsdorf, R. Festag, J. H. Wendorff, P. A. Heiney and N. C. Maliszewskyj, *Liq. Cryst.*, 1995, **19**, 759–764.
41 V. Percec, G. Johansson, G. Ungar and J. Zhou, *J. Am. Chem. Soc.*, 1996, **118**, 9855–9866.
42 M. Campos-Vallette and M. Rey-Lafon, *J. Mol. Struct.*, 1983, **101**, 23–45.
43 N. Terasawa, H. Monobe and K. Kiyohara, *Liq. Cryst.*, 2007, **34**, 311–324.
44 V. Percec, D. Schlueter, Y. K. Kwon, J. Blackwell, M. Moeller and P. J. Slangen, *Macromolecules*, 1995, **28**, 8807–8818.

45 J. Dai, K.-Q. Zhao, B.-Q. Wang, P. Hu, B. Heinrich and B. Donnio, *J. Mater. Chem. C*, 2020, **8**, 4215–4225.
46 N. Godbert, A. Crispini, M. Ghedini, M. Carini, F. Chiaravalloti and A. Ferrise, *Appl. Crystallogr.*, 2014, **47**, 668–679.
47 P. Ehni, K. Guy, M. Ebert, S. Beardsworth, K. Bader, R. Forschner, A. Bühlmeyer, N. Dumait, C. Roiland and Y. Molard, *Dalton Trans.*, 2018, **47**, 14340–14351.
48 S. K. Prasad, D. S. Rao, S. Chandrasekhar and S. Kumar, *Mol. Cryst. Liq. Cryst.*, 2003, **396**, 121–139.
49 K. Shizu and H. Kaji, *Commun. Chem.*, 2022, **5**, 53.
50 T. Hatakeyama, K. Shiren, K. Nakajima, S. Nomura, S. Nakatsuka, K. Kinoshita, J. Ni, Y. Ono and T. Ikuta, *Adv. Mater.*, 2016, **28**, 2777–2781.
51 A. Pershin, D. Hall, V. Lemaur, J.-C. Sancho-Garcia, L. Muccioli, E. Zysman-Colman, D. Beljonne and Y. Olivier, *Nat. Commun.*, 2019, **10**, 597.
52 F. Würthner, T. E. Kaiser and C. R. Saha-Möller, *Angew. Chem., Int. Ed.*, 2011, **50**, 3376–3410.
53 S. Ma, S. Du, G. Pan, S. Dai, B. Xu and W. Tian, *Aggregate*, 2021, **2**, e96.
54 D. Hall, S. M. Suresh, P. L. dos Santos, E. Duda, S. Bagnich, A. Pershin, P. Rajamalli, D. B. Cordes, A. M. Slawin and D. Beljonne, *Adv. Opt. Mater.*, 2020, **8**, 1901627.
55 J. Park, J. Lim, J. H. Lee, B. Jang, J. H. Han, S. S. Yoon and J. Y. Lee, *ACS Appl. Mater. Interfaces*, 2021, **13**, 45798–45805.
56 R. Keruckiene, A. A. Vaitusionak, M. I. Hulnik, I. A. Berezianko, D. Gudeika, S. Macionis, M. Mahmoudi, D. Volyniuk, D. Valverde and Y. Olivier, *J. Mater. Chem. C*, 2024, **12**, 3450–3464.
57 X. Wu, B.-K. Su, D.-G. Chen, D. Liu, C.-C. Wu, Z.-X. Huang, T.-C. Lin, C.-H. Wu, M. Zhu and E. Y. Li, *Nat. Photonics*, 2021, **15**, 780–786.
58 H. Uoyama, K. Goushi, K. Shizu, H. Nomura and C. Adachi, *Nature*, 2012, **492**, 234–238.
59 D. Sun, S. M. Suresh, D. Hall, M. Zhang, C. Si, D. B. Cordes, A. M. Slawin, Y. Olivier, X. Zhang and E. Zysman-Colman, *Mater. Chem. Front.*, 2020, **4**, 2018–2022.
60 D. Sun, E. Duda, X. Fan, R. Saxena, M. Zhang, S. Bagnich, X. Zhang, A. Köhler and E. Zysman-Colman, *Adv. Mater.*, 2022, **34**, 2110344.
61 J. M. dos Santos, D. Sun, J. M. Moreno-Naranjo, D. Hall, F. Zinna, S. T. Ryan, W. Shi, T. Matulaitis, D. B. Cordes and A. M. Slawin, *J. Mater. Chem. C*, 2022, **10**, 4861–4870.
62 A. C. Chen, S. W. Culligan, Y. Geng, S. H. Chen, K. P. Klubek, K. M. Vaeth and C. W. Tang, *Adv. Mater.*, 2004, **16**, 783–788.
63 C.-P. Han, E. H.-C. Shi, C. A. Chen, C.-H. Hsu, C.-H. Chen, C.-C. Wu, Y.-T. Lee, T.-L. Chiu, J.-H. Lee and M. Leung, *Adv. Opt. Mater.*, 2024, **12**, 2303295.
64 M. Yang, I. S. Park and T. Yasuda, *J. Am. Chem. Soc.*, 2020, **142**, 19468–19472.
65 K. Stavrou, A. Danos, T. Hama, T. Hatakeyama and A. Monkman, *ACS Appl. Mater. Interfaces*, 2021, **13**, 8643–8655.
66 T. Förster, *Ann. Phys.*, 1948, **437**, 55–75.
67 S.-H. Liu, M.-S. Lin, L.-Y. Chen, Y.-H. Hong, C.-H. Tsai, C.-C. Wu, A. Poloek, Y. Chi, C.-A. Chen and S. H. Chen, *Org. Electron.*, 2011, **12**, 15–21.
68 Y. Wu, C. Yan, X.-S. Li, L. H. You, Z.-Q. Yu, X. Wu, Z. Zheng, G. Liu, Z. Guo and H. Tian, *Angew. Chem.*, 2021, **133**, 24754–24762.
69 S. Wu, Y.-N. Hu, D. Sun, K. Wang, X.-H. Zhang and E. Zysman-Colman, *Chem. Commun.*, 2024, **60**, 2489–2492.
70 S. Wu, Y.-N. Hu, J. Wang, D. Sun, K. Wang, X.-H. Zhang and E. Zysman-Colman, *J. Mater. Chem. C*, 2024, **12**, 6177–6184.
71 S. Wu, A. Kumar Gupta, K. Yoshida, J. Gong, D. Hall, D. B. Cordes, A. M. Slawin, I. D. Samuel and E. Zysman-Colman, *Angew. Chem., Int. Ed.*, 2022, **61**, e202213697.
72 W. Pisula, M. Kastler, D. Wasserfallen, J. W. Robertson, F. Nolde, C. Kohl and K. Müllen, *Angew. Chem., Int. Ed.*, 2006, **45**, 819–823.
73 T. Wöhrle, H. Taing, C. Schilling, S. H. Eichhorn and S. Laschat, *Liq. Cryst.*, 2019, **46**, 1973–1984.
74 E. O. Arikainen, N. Boden, R. J. Bushby, O. R. Lozman, J. G. Vinter and A. Wood, *Angew. Chem.*, 2000, **112**, 2423–2426.

